Journal of Thermal Analysis and Calorimetry, Vol. 79 (2005) 595–604

THERMOANALYTICAL AND STRUCTURAL PROPERTIES OF METAL OXIDE SEMICONDUCTOR AND PALLADIUM/LAYER SILICATE NANOCOMPOSITES

R. Kun[1], *K. Mogyorósi*[1], *J. Németh*[2], *L. Kőrösi*[2], *Sz. Papp*[2] *and I. Dékány*[1,2*]

[1]Department of Colloid Chemistry, University of Szeged, Aradi v. t. 1, 6720 Szeged, Hungary
[2]Nanostructured Materials Research Group of the Hungarian Academy of Sciences, University of Szeged, Aradi v. t. 1 6720 Szeged, Hungary

The thermoanalytical and structural properties of composites of layer silicates with metal oxide semiconductors (TiO_2, ZnO and SnO_2) prepared by adsorption and heterocoagulation (sol/gel technology) were studied. In addition to metal oxides, the intercalation of nanoparticles of noble metal, palladium was also investigated using the above experimental technique. It was established that the incorporation of nanoparticles into the layered structure is adequately described by thermoanalytical data. When metallic palladium nanoparticles are stabilized by surfactants and macromolecules, heat decomposition of the stabilizers within the nanocomposite can also be detected. Thermoanalytical data were combined with X-ray diffraction and transmission electron microscopic information to verify the composition of the composites. Changes in the nanoparticle content of the composites were also confirmed by structural studies.

Keywords: *nanoparticles, palladium, semiconductors, thermogravimetry, X-ray diffraction*

Introduction

The preparation of titanium dioxide has been addressed by a great number of publications. The majority of these describe titanium dioxide products prepared via controlled hydrolysis of titanium(IV) alkoxides [1]. In the course of hydrolysis, the reaction partner of the titanium precursor is water, which is, in most cases, also the main component of the reaction medium (alcohol/water mixture). There are many reports in the literature on the preparation and evaluation of composites containing titanium dioxide. The properties of supported materials and composites are more favourable for practical utilization than those of pure titanium dioxide. Layer silicates are widely used supports [2–5]. Layer silicates are also eminently suitable for the preparation of particles with a diameter of a few nanometers on the surface and in the interlamellar space of clays in aqueous suspensions. Particle growth within the interlamellar space is sterically hindered. Sterte *et al*. [2] prepared titanium hydroxide by acid hydrolysis of titanium(IV) chloride and added it to a suspension of montmorillonite. The products studied exhibited a very low degree of crystallinity: X-ray diffractograms showed evidence for the onset of the formation of an anatase phase. Calcination at higher temperatures (750°C) resulted in the crystallization of the anatase phase without the appearance of a rutile phase. The value of basal spacing as derived from the position of Bragg reflexion *d*(001) measured at small scattering angles is 3.4 nm before and 2.8–3.0 nm after calcination. The specific surface area of non-calcined composites varied between 220 and 335 $m^2\ g^{-1}$, calcination brought about a considerable decrease in specific surface area (100–150 $m^2\ g^{-1}$), especially at temperatures above 700°C.

Colloidal chemical techniques have been widely used to prepare the ZnO particles in the nanoscale regime: sol-gel method [6, 7], phase transfer technique [8], hydrolysis of chelate complex [9], polymer stabilization [10], synthesis in reversed micelles [11] and alkoxide based process [12]. In the present work ZnO nanoparticles were synthesized in aqueous medium, using montmorillonite layered silicate (clay mineral) as stabilizer and support of the nanocrystals.

Due to its favourable physical and chemical properties, tin dioxide has multiple practical applications including the construction of semiconductors, resistors, electrodes and chemical sensors [13, 14] and, since it is photocatalytically active, it may also be used for the degradation of organic compounds [15]. Its favourable properties are closely linked to particle size.

Particle size may be stabilized by layer silicates, whose interlamellar distance makes possible the preparation of particles of a well-defined size (3–6 nm) [16–18]. The method involves coagulation of a sol

* Author for correspondence: i.dekany@chem.u-szeged.hu

1388–6150/$20.00

Akadémiai Kiadó, Budapest, Hungary
Springer, Dordrecht, The Netherlands

with positive surface charge and a layer silicate suspension with negative surface charge, which is why the method is known as heterocoagulation [19].

The most commonly used stabilizing agents for nanoparticle preparation are surfactants, polymers with the help of which sols containing particles of subcolloid size are synthetized.

Metal particles are most conveniently grown on the clay mineral surface by displacing the exchangeable cation by precursor transition metal cations and by subsequent reduction. In our earlier works the adsorption layer at the solid/liquid interface was employed as a 'nanophase reactor' for the generation of nanocrystalline metal particles and for their stabilization in the presence of the clay mineral [20, 21]. The nanoparticles can be grown attached to the surface, in well controllable number and size between the silicate layers. In view of the powerful stabilizing effect of polymers, we set out to test the joint stabilizing effect of the polymer/clay mineral complex in the preparation of Pd^0 nanoparticles. We showed that monodisperse particles can be obtained, the size of which depends on polymer and precursor ion concentrations and on the chemical nature of the reducing agent used [22, 23].

In the present work, nanoparticles were prepared using two different methods. The first of these was the so-called controlled colloid synthesis (CCS), i.e. the generation of nanoparticles within the adsorption layer on the surface of the support, functioning as a nanophase reactor, via reduction or hydrolysis [2, 9, 22, 23]. The second method was heterocoagulation: nanosize (2–10 nm) metal or metal hydroxide colloid (sol) particles are prepared in a separate experiment and are subsequently coagulated with layer silicates of the opposite surface charge [2–5, 19]. In both cases nanoparticles are intercalated between the lamellae of layer silicates, a process that yields structurally well controllable nanoparticle/layer silicate composites [16–18, 20, 21].

Experimental procedures

Materials

Supports for the preparation of nanoparticles in various composite samples were layer silicates (Na-montmorillonite and synthetic hectorite (Optigel SH), Südchemie AG, Munich, Germany). Nanoparticles were prepared from salts of the corresponding metals or from organic precursors. TiO_2 nanoparticles were synthesized starting from titanium(IV) isopropoxide (Fluka Chemical, pract.) in high-purity water (Millipore Co., 18 MΩ cm) and 2-propanol (Reanal, Hungary, puriss.) as medium. pH was adjusted with concentrated hydrogen chloride solution (Reanal, Hungary, p.a.), which was also used as a reagent. ZnO nanoparticles were prepared from zinc chloride (Reanal, Hungary, puriss.).

For the preparation of the SnO_2 nanoparticles tin(IV) chloride pentahydrate (minimal purity 98%, Aldrich Chem. Co.) was used.

The metal precursor palladium(II) chloride (purity 99%) was obtained from Aldrich. A polymer was used to stabilize the Pd nanoparticles: poly(N-vinyl-2-pyrrolidone) (PVP, K–30, average molecular mass $4 \cdot 10^4$ g, Fluka) and octylamine (purity 99%, Fluka) were used as protective agents for the Pd nanoparticles. Methanol (Reanal, Hungary) was of analytical purity. Dimethyl sulphoxide (DMSO, analytical purity, Reanal, Hungary) was used for delamination of the kaolinite particles. The reducing agent hydrazine (purity 99%) was obtained from Aldrich. Fine fraction ($d \leq 2$ μm) of kaolinite (Zettlitz, Germany) was used as support for the preparation of nanoparticles.

Sample preparation

Preparation of TiO_2/montmorillonite composites

Titanium hydroxide sols were prepared from the alcoholic solution of titanium(IV) isopropoxide by acid hydrolysis. A mixture of 174 mL of titanium(IV) isopropoxide+146 mL of 2-propanol is added to 660 mL of Milli-Q water under vigorous stirring. 18 mL of concentrated hydrochloric acid is next added dropwise to the white dispersion. The continuously stirred solution is thermostated at 50±2°C and stirring is continued for 12 h at this temperature. By the end of the incubation the $Ti(OH)_4$ sol clears up and has a pH of 1.0. The pH of the sol is adjusted to 4.0 by the addition of 1 mol dm^{-3} NaOH solution, the sol is diluted with distilled water and centrifuged. The precipitate is twice washed with distilled water. The volume of the washed precipitate is made up to the original volume and the pH of the medium is again adjusted to 4.0.

For heterocoagulation, washed $Ti(OH)_4$ sol (pH=4.0) was used. The semiconductor contents of the composites were 20, 33, 50, 66 and 75% (mass%). For composite preparation, the sol was added dropwise to a Na-montmorillonite suspension, which took 30 min in all cases. The composite suspensions obtained were left to settle for 20 h, washed in distilled water and centrifuged in a Sorvall centrifuge for 30 min at 11,000 rpm. The sediment was dried at 50°C and the dried material was pulverized in an agate mortar.

Synthesis of ZnO/montmorillonite by the preadsorption method

To 4·20 mL of 0.5 mol dm^{-3} zinc chloride solution, 20, 10, 5 and 0 mL, respectively, of 1.0 mol dm^{-3} hy-

drochloric acid solution was added. The volume of each of the four samples was next made up to 175 mL by the addition of Milli-Q water and to each vessel 25 mL of 4% aqueous montmorillonite suspension was added under constant stirring. After a reaction time of 3 h the suspensions were centrifuged and washed in distilled water several times, until no more prepcipitate was formed on addition of silver nitrate to the supernatant. The sediment was dried in a drying cabinet at 80°C. Portions of each of the four samples were next calcined at 400°C in a tube furnace. The zinc oxide content of the nanocomposites was determined after acid digestion, by complexometric titration of Zn^{2+} ions with methyl thymol blue as indicator.

Preparation of SnO_2/layer silicate composites

$Sn(OH)_4$ hydrosols were prepared by hydrolysis of $SnCl_4$ using the following procedure: 4.75 g of $SnCl_4 \cdot 5H_2O$ and 1.06 g of NaOH were dissolved into 50.0 mL distilled water each. The alkali solution was added dropwise to the vigorously stirred tin(IV) chloride solution and the mixture was homogenized by sonication for 5 min. For the preparation of nanocomposites, tin(IV) hydroxide sol (water:sol=1:1; Sn(OH)4 ~ $3.3 \cdot 10^{-2}$ mol dm^{-3}) was used. Tin dioxide nanoparticles were delivered to the interlamellar space by heterocoagulation, when different amounts of $Sn(OH)_4$ sol were added to 1 (mass/*v*)% montmorillonite or hectorite suspensions under constant stirring. The resulting $Sn(OH)_4$/layer silicate nanocomposite suspensions were centrifuged for 15 min at 3500 min^{-1}. The sediment was redispersed in ca. 400 mL distilled water, washed and recentrifuged. The product was washed three times in distilled water and once in ethanol, dried at 80°C and ground to a fine powder in an agate mortar. The samples were calcinated in a tube furnace (heating rate 5°C min^{-1}) for 3 h at 400°C.

Preparation of Pd/kaolinite/PVP composites

The kaolinite was expanded by the intercalation of DMSO at *T*=65°C. The excess of DMSO was removed from the sample by several washing with methanol within 5 days. Pd/kaolinite complexes were prepared, directly by reduction of Pd^{2+} ions 0.7 mmol dm^{-3} concentration aquatic solution previously adsorbed in the MeOH/DMSO/kaolinite system and, on the other, by applying a polymer and surfactant to ensure binding to the lamellae and steric stabilization. Macromolecules were adsorbed on the support from a methanol or aquatic solution which was followed by adsorption and reduction of Pd^{2+} ions. Intercalation complexes of nonionic polyvinylpyrrolidone(PVP)/kaolinite were prepared by this method in systems containing various (0.1–2.0 mass%) concentrations of methanol/PVP, or water/PVP, by polymer adsorption. Intercalation complexes of octylamine/kaolinite (0.12–1.2 g octylamine/1 g kaolinite) were prepared at pH=4.0 in system containing various (0.5–0.05 mol dm^{-3}) concentration of water/octylamine. 1 g of MeOH/DMSO/kaolinite intercalation compound were dispersed in 20 mL solution of polymer or surfactant, and the mixtures were stirred at room temperature for 24 h. The metal content of the products was 0.45–1.4 mass%.

Measurement methods

The XRD experiments were carried out in a Philips X-ray diffractometer (PW 1930 generator, PW 1820 goniometer) with CuK_α radiation (λ=0.15418 nm). The basal spacing (d_L) was calculated from the (001) reflection via the Bragg equation.

In the course of our thermoanalytical studies, temperature (*T*), change in mass (TG) and change in enthalpy (DTA) were measured in dynamic mode, in the temperature range of 25–1000°C. Measurements were carried out in air in a type Q-1500 D MOM Derivatograph, applying a heating rate of 5°C min^{-1}. The samples (100 mg each) were placed in ceramic crucibles. The reference was α-Al_2O_3. The results were evaluated with the help of a computer program.

Results and discussion

The metal oxide/layer silicate composites

A prerequisite of the interpretation of thermoanalytical measurements is information regarding composite structure. Sample analysis was therefore started with XRD studies. Samples dried at 50°C, containing 20, 33, 50, 66 or 75 mass% titanium dioxide were subjected to X-ray diffraction analysis at both small (2θ=1–15°) and large (2θ=20–30°) scattering angles. Reflexions falling into the small angle range confirm the intercalation structure of nanocomposites, whereas those in the large angle range are characteristic of the structure of titanium dioxide. Small angle X-ray diffractograms of the composites compared to that of the original Na-montmorillonite are shown in Fig. 1a. Values of d_L shown on the diffractograms indicate the average basal spacing of Na-montmorillonite and the pillared nanocomposite. The characteristic reflexion of pure Na-montmorillonite appears at 2θ=7.5°. The intensity of this reflexion decreases with increasing titanium dioxide content and is quite low in the sample containing 50 mass% TiO_2. The parallel appearance of the Bragg reflexion characteristic of intercalation structure is observed at about 2θ=2.0°, demonstrating

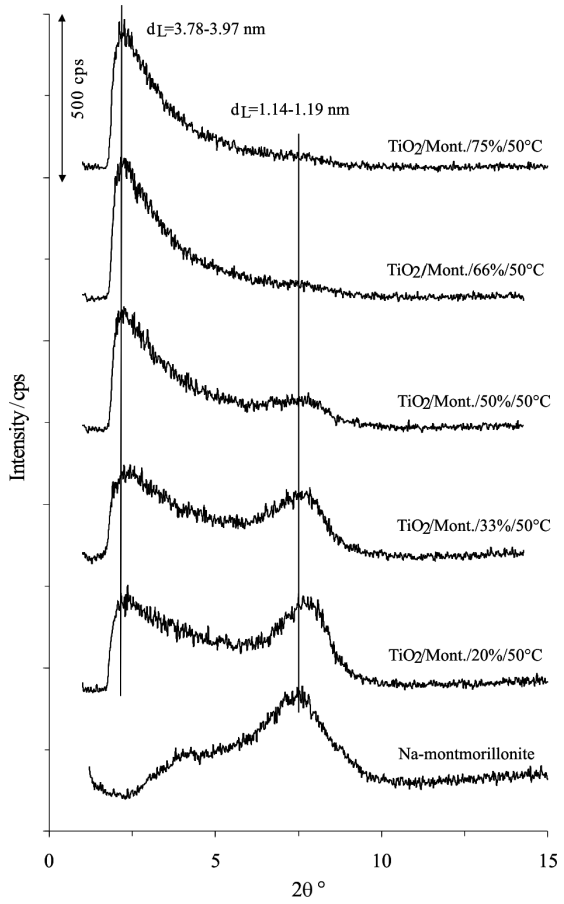

Fig. 1a XRD patterns of Na-montmorillonite and their composites prepared with dialyzed $Ti(OH)_4$ nanosols at pH=4.00 (at small angle region)

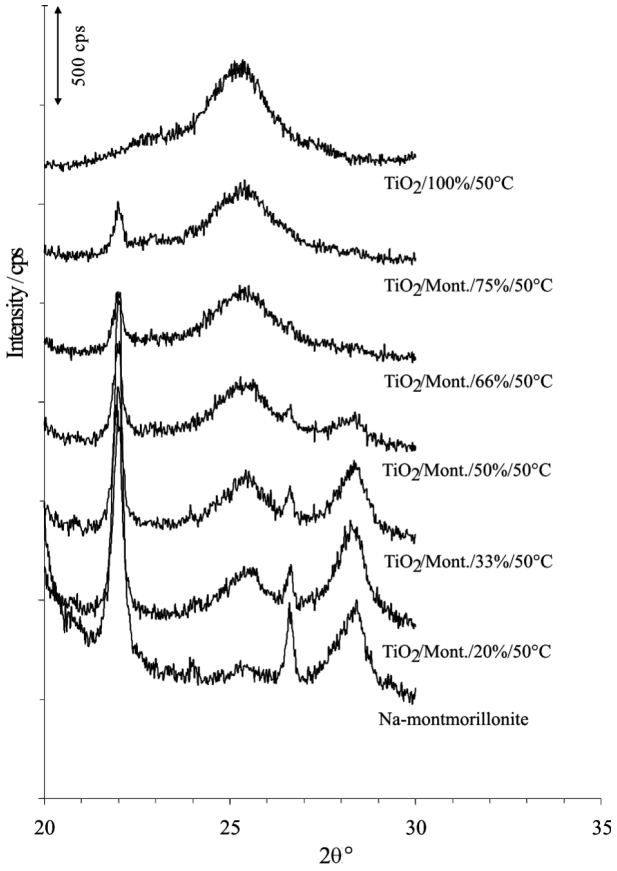

Fig. 1b XRD patterns of Na-montmorillonite and their composites prepared with dialyzed $Ti(OH)_4$ nanosols at pH=4.00 (at high angle region)

the incorporation of titanium dioxide nanoparticles in the interlamellar space. The intensity of this reflexion gradually increases with increasing titanium dioxide content. On the basis of the position of these reflexions, the height of TiO_2 pillars is 2.8–3.0 nm: this value can be calculated from the experimentally determined basal spacing and the thickness of the TOT (tetrahedral-octahedral-tetrahedral) layer of the clay mineral montmorillonite (0.96 nm) ($d_{TiO_2} = d_L - d_{TOT}$). Values of d_L for TiO_2/Na-montmorillonites reported in the literature are all considerably lower (d_L=2–2.8 nm), which may be explained by the fact that particles incorporated by methods other than heterocoagulation are smaller and non-crystalline. Measurements in the angle range of 2θ=20–30° yield the diffractograms presented in Fig. 1b. The peak appearing at about 2θ=25° is characteristic of the anatase modification of titanium dioxide. The average diameter of anatase particles determined by the Scherrer equation is 4.1–4.6 nm. The other reflexions appearing on the diffractogram are characteristic of montmorillonite and its accompanying minerals and, naturally, their intensity decreases with decreasing Na-montmorillonite content.

Thermoanalytical measurements indicated a temperature range of 300–400°C for the formation of anatase (the crystalline modification of titanium dioxide, TiO_2) from titanium hydroxide prepared by the hydrolysis of titanium tetraisopropoxide. Calcination of titanium hydroxide is a multistep polycondensation process [24].

Sample TiO_2/100%/50°C, obtained by hydrolysis of titanium(IV) isopropoxide in 2-propanol was X-ray amorphous; it was therefore subjected to thermoanalysis to determine the temperature of the appearance of an anatase phase. By the evidence of the TG curve shown in Fig. 2, the chemical formula of sample TiO_2/100%/50°C is $Ti(OH)_4$ (or $TiO_2 \cdot 2H_2O$), the composition matching the mass change taking place up to 400°C (31%). Amorphous $TiO_2 \cdot 2H_2O$ xerogel is converted to titanium dioxide in a series of polycondensation steps. The process, accompanied by the elimination of water, is endothermic in the temperature range of 25–200°C (see the peak at 114.2°C on the DTA curve), and is followed by an exothermic process at 200–400°C (313.5°C). According to our X-ray diffraction measurements, this is the step when amorphous titanium dioxide is converted to anatase phase titanium

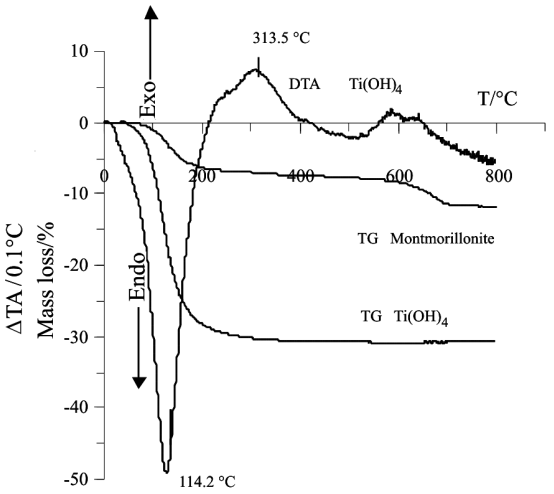

Fig. 2 TG and DTG curves of Na-montmorillonite and $Ti(OH)_4$ (synthesized from Ti-alkoxide, drying at 50°C, without calcination)

dioxide. The DTA curve also reveals a further exothermic process between 500 and 750°C, corresponding to the anatase-rutile phase transition. All this means that in our samples prepared by similar methods, the appearance and prevalence of a pure anatase phase may be expected in the temperature range of 320–500°C. Figure 2 also includes the thermogravimetric curve of Na-montmorillonite, characterized by two significant steps of mass loss. In the first step, adsorbed water evaporates from the lamellae (dehydration, 25–200°C), whereas in the second step structural water leaves the silicate skeleton (dehydroxylation, 550–700°C). This means that, in order to generate anatase phase without serious damage to mineral structure, TiO_2-montmorillonite samples should be calcined at 320–400°C.

TG curves of TiO_2/Na-montmorillonite composite samples show evidence for large mass losses (nearly 10%) up to 200°C. This is the stage of dehydration, in the course of which the samples lose water adsorbed in their pores and on their internal and external surfaces. These processes are also clearly observed on the DTA curves (Fig. 3), where the individual transitions are indicated by the appearance of endothermic peaks. At 200–500°C the amorphous fraction of the $TiO_x(OH)_y$ content of the samples is totally converted to TiO_2 and it is also in this temperature range that TiO_2 particles are sintered. For both composites and Na-montmorillonite, another significant mass loss is observed at 550–700°C, which is attributable to the dehydroxylation of Na-montmorillonite, and whose magnitude therefore decreases with increasing titanium dioxide content.

Titanium dioxide/montmorillonite complexes behaved differently from simple TiO_2 samples. DTA measurements failed, up to 1000°C, to reveal any evidence for the anatase to rutile phase transition. In con-

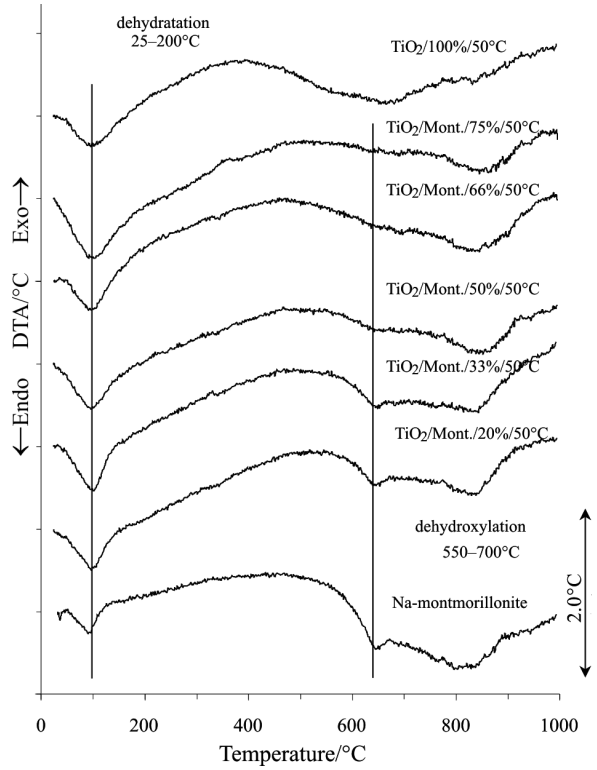

Fig. 3 DTA curves of Na-montmorillonite and their composites prepared with $Ti(OH)_4$ nanosols and dried at 50 °C

trast, in physical powder mixtures of montmorillonite and TiO_2 90% of the latter underwent transformation to rutile upon heating to 800°C, as evidenced by the presence of an XRD peak at 2θ=27.5° (Fig. 4). In the case of the TiO_2/Na-montmorillonite composite, reflexions of more and more smaller half-width are obtained at 2θ=25.2° with increasing calcination temperature, indicating that the proportion of crystalline anatase phase increases with the simultaneous formation of only insignificant amounts of rutile phase.

In order to convert the zinc hydroxide particles formed in the course of synthesis to zinc oxide, a heat treatment has to be performed. After calcination of ZnO/Na-montmorillonite composites at 400°C, their

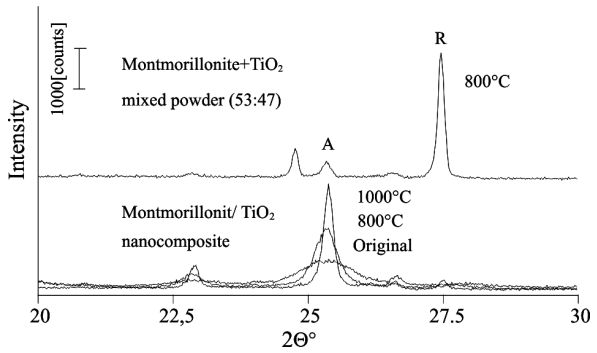

Fig. 4 XRD patterns of TiO_2/montmorillonite nanocomposite catalyst after calcination

Table 1 Properties of semiconductor/clay mineral nanocomposites

Sample	Metal-oxide content/mass%	Basal spacing, d_L/nm	Particle diameter/nm
Na-montmorillonite	–	1.21	–
Na-hectorite	–	1.19	–
TiO_2/Mont./20%/50	20		
TiO_2/Mont./33%/50	33		
TiO_2/Mont./50%/50	50	3.78–3.97	2.82–3.01
TiO_2/Mont./66%/50	66		
TiO_2/Mont./75%/50	75		
TiO_2/100%/50	100		
ZnO/Mont./7.7%/400	7.7	1.68	0.72
ZnO/Mont./14.9%/400	14.9	2.12	1.16
ZnO/Mont./16.2%/400	16.2	3.40	2.44
ZnO/Mont./21.0%/400	21.0	5.63	4.67
SnO_2/Mont./14.4%/400	14.4	6.6	5.64
SnO_2/Mont./26.0%/400	26.0	3.5	2.54
SnO_2/Mont./40.9%/400	40.9	2.7	1.74
SnO_2/Hect./30.6%/400	30.6	6.1	5.14
SnO_2/Hect./50.3%/400	50.3	3.3	2.34

X-ray diffractograms were recorded (Fig. 5). Basal spacing values characteristic of the original structure of Na-montmorillonite can be observed at 2θ=9.3° in every sample. In the course of the intercalation of ZnO nanoparticles into the interlamellar space, however, the structure of the clay mineral is altered and an increase in basal spacing is evinced by the appearance of a new reflexion at smaller angles (2θ=1–5°). Basal spacing after intercalation is expressly dependent on the amount of ZnO incorporated in the course of synthesis (Table 1). The average diameter of intercalated nanoparticles derived, from values of basal spacing, falls in the range of 1–4 nm, depending on the conditions of preparation.

DTA curves of ZnO-montmorillonite nanocomposites are presented in Fig. 6. The mass loss manifesting itself in the DTA curves is a result of the evaporation of the water content of the samples. Three stages of the process can be discerned. In the first step, up to 100°C physically bound water is removed, whereas the subsequent steady mass loss is a sign of dehydration accompanying the conversion $Zn(OH)_2 \xrightarrow{-H_2O} ZnO$. Finally, at 600–700°C loss of the structural water of montmorillonite commences, resulting in the collapse of clay mineral structure. All DTA curves have a minimum at 100°C, indicating the heat absorption necessary for the evaporation of physically adsorbed water. The curves then start to rise in the

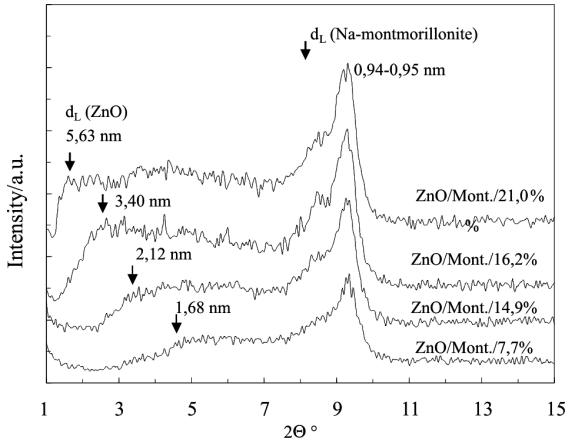

Fig. 5 XRD patterns of ZnO/Na-montmorillonite composites prepared from $ZnCl_2$ solution and Na-montmorillonite suspension

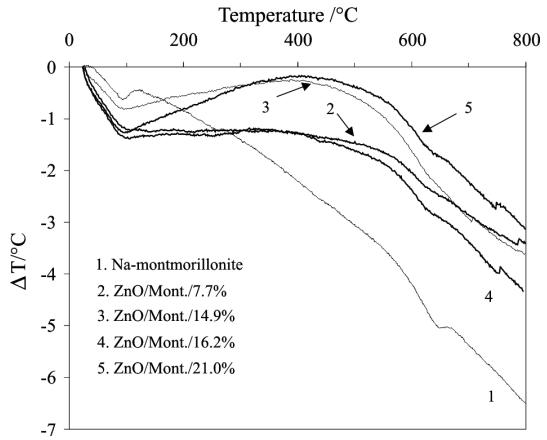

Fig. 6 DTA curves of ZnO/Na-montmorillonite composites prepared from $ZnCl_2$ solution and Na-montmorillonite suspension

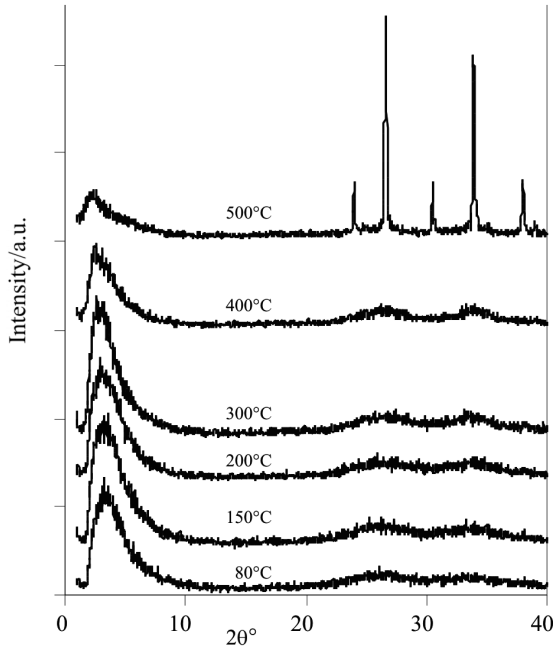

Fig. 7 XRD patterns of SnO_2/Hect./50.3% nanocomposites calcinated at different temperatures

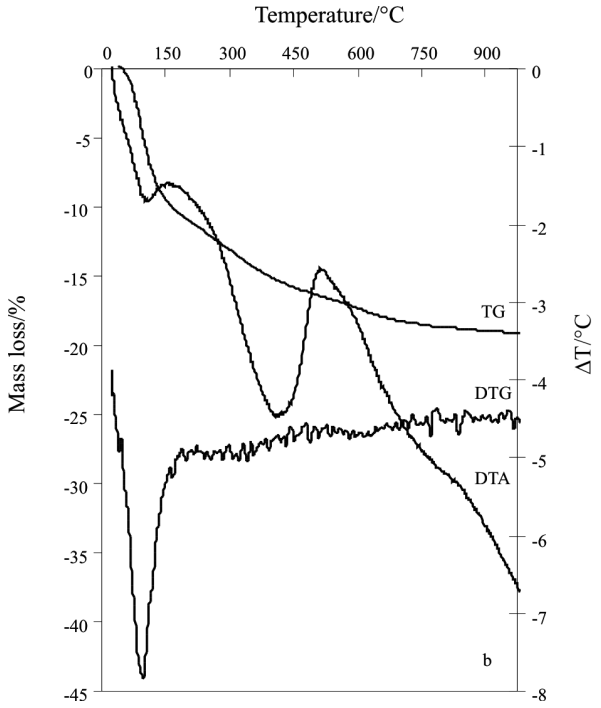

Fig. 8 Thermoanalytical measurements of SnO_2/Hect./50.3% nanocomposite

exothermic direction, which is attributable to the heat released in the course of the crystallization of nascent ZnO particles, partially balancing heat absorption due to the ongoing water loss. The tendency of the curves to turn endothermic above 500°C is indicative of the enthalpy need of the dehydroxylation of montmorillonite. In the case of the 'empty' montmorillonite support containing no nanoparticles, however, sample temperature as compared to that of the control decreases essentially constantly, suggesting that no heat-generating crystallization processes like those operating in zinc oxide containing systems take place. The above observations allow to conclude that the ideal temperature for calcination is around 400°C, because the $Zn(OH)_2 \xrightarrow{-H_2O} ZnO$ conversion is completed below this temperature, whereas temperatures above 600°C already promote the dehydroxylation of the support.

The intercalation of nanoparticles alters the original basal spacing of hectorite. Increasing the tin content of the sample also brings about a decrease in basal spacing, because adding more and more $Sn(OH)_4$ sol to the layer silicate suspension the pH of the formed $Sn(OH)_4$/layer silicate disperse system decreases, causing the presence of the smaller semiconductor nanocrystals (Table 1). Calcination temperature also plays a role in the changes occurring in the structure of layer silicates. The effect of temperature on mineral structure was studied in detail on the SnO_2/Hect./50.3% sample (Fig. 7). In samples heated to higher temperatures the intercalation peak is more diffuse, its intensity decreases, whereas the peaks characteristic of SnO_2 appear at progressively increasing intensities and decreasing half widths, indicating structural degradation of the support as well as an increase in the crystallinity of tin dioxide.

The SnO_2/Hect./50.3% nanocomposite was subjected to thermoanalytical studies, the results of which are shown in Fig. 8. By the evidence of the DTG curve, the joint dehydration of the metal hydroxide and the mineral takes place between 100 and 190°C; in the region from 290 to 520°C, a slight decrease in mass indicates the hydroxide→oxide conversion (minimum at 340°C). Between 570 and 690°C, another slight but detectable mass loss signals the dehydroxylation of hectorite (minimum at 630°C). The above processes may also be recognized in the different regions of the DTA curve. It has to be noted that the second endothermic process is followed by an exothermic one, crystallization of amorphous tin oxide, which may be verified in an independent experiment.

The palladium/kaolinite composites

In order to create the space necessary for the synthesis of nanoparticles, the hydrogen bonds tightly interlinking the kaolinite layers must be broken up. As indicated by XRD experiments interlamellar expansion was nearly 100% after the formation of the DMSO/kaolinite intercalation complex. The basal spacing increased from 0.72 to 1.12 nm within 24 h (Figs 9a, b). The interlamellar distance was unchanged after removal excess of DMSO. Kaolinite containing palladium were pre-

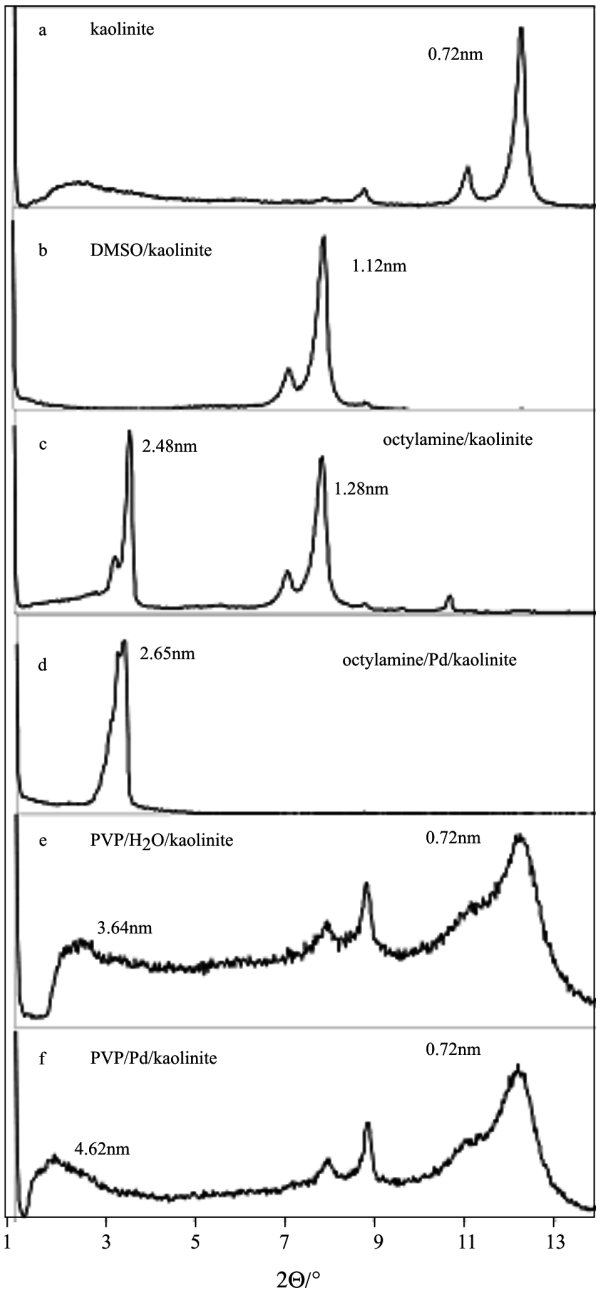

Fig. 9 XRD patterns of kaolinite samples, a – pure kaolinite; b – DMSO/kaolinite intercalation complex; c – octylamine/kaolinite intercalation complex; d – palladium (1 mass%) /octylamine/kaolinite nanocomposite; e– PVP/kaolinite and; f– palladium (1 mass%)/PVP/kaolinite nanocomposite

pared using octylamine in acidic medium (pH=4.0) to separate the silicate layers. The amount of octylamine was 0.2 g/1g kaolinite. The reflection at d_L=2.48 nm indicates the intercalation of octylammonium ions in addition the reflection at d_L=1.28 nm characteristic of the DMSO/kaolinite intercalation complex shifted from d_L=1.12 nm (Fig. 9c). In the course of reduction by hydrazine following the adsorption of palladium ions, a further shift of the 001 reflection was observed (2.65 nm) (Fig. 9d).

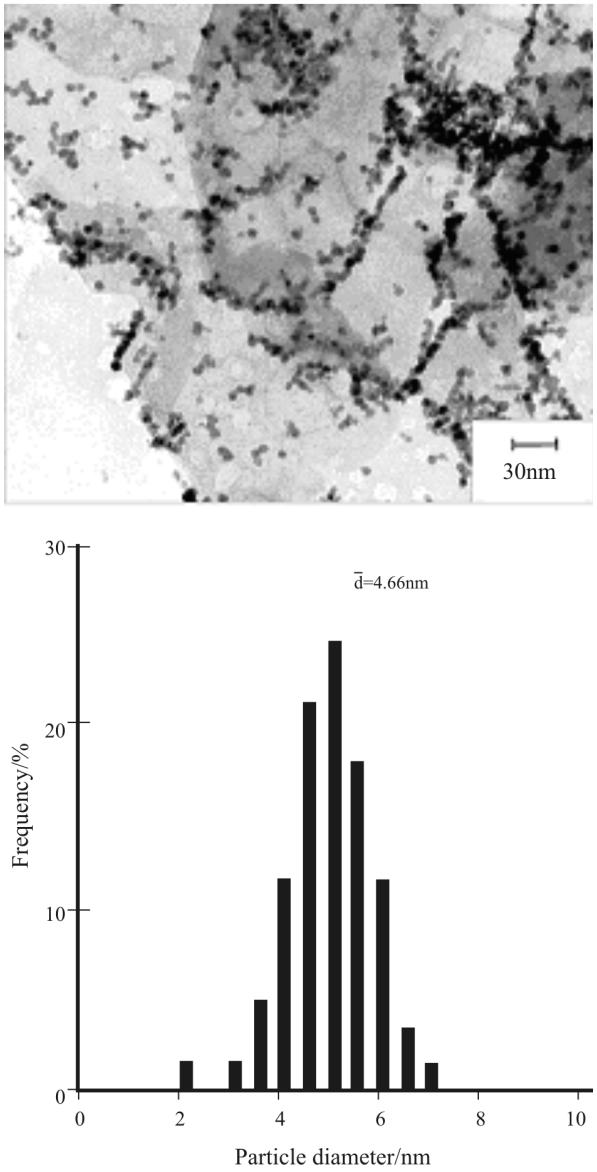

Fig. 10 TEM image of Pd (1 mass%)/PVP (3.8 mass%)/kaolinite composites

For synthesis applying macromolecules were first adsorbed on the support from aqueous solution. When 1 (mass/*v*)% aqueous PVP solution was contacted with kaolinite, the peak characteristic of the intercalation compound of kaolinite was not observed. Rather, the initial (001) reflection reappeared and a broadened peak of d_L~3.6 nm was observed (Fig. 9e). This indicates that in contact with the aqueous PVP solution a part of the kaolinite layers reaggregate whereas the remaining layers adsorb PVP. Formation of metal clusters in the interlamellar space was indicated by a shift of reflection from d_L=3.6 to d_L=4.6 nm (Fig. 9f).

The TEM image of the Pd/PVP/kaolinite composite shows spherical particles with diameters of 2–4 nm, separately, without aggregation attached to the lamellae (Fig. 10). Electron micrographs of the complexes con-

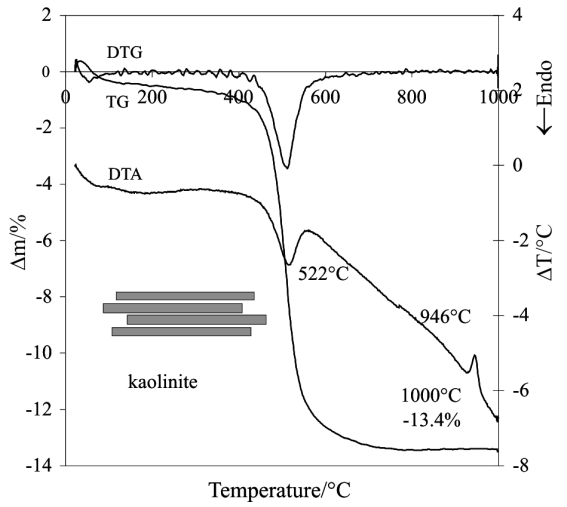

Fig. 11a The TG/DTG and DTA curves of pure kaolinite

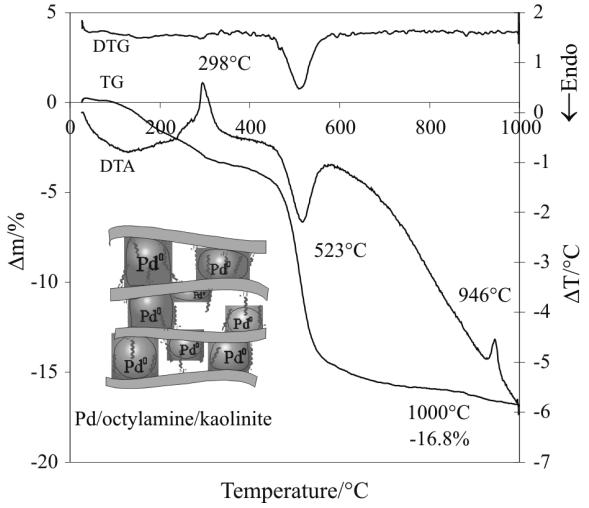

Fig. 12a The TG/DTG and DTA curves of palladium (1 mass%)/ octylamine/kaolinite intercalation complex

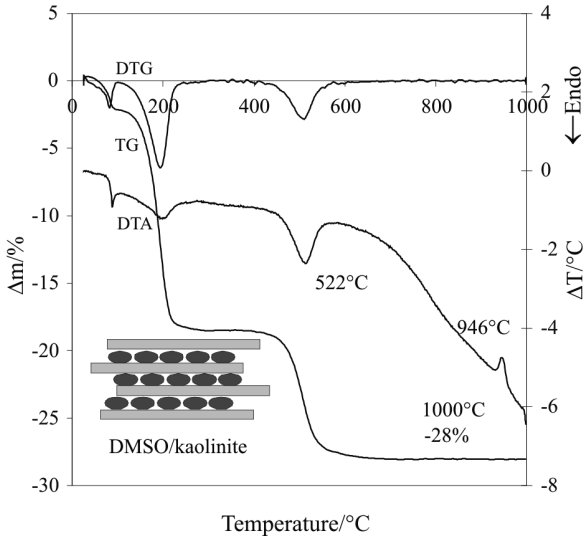

Fig. 11b The TG/DTG and DTA curves of DMSO/kaolinite intercalation complex

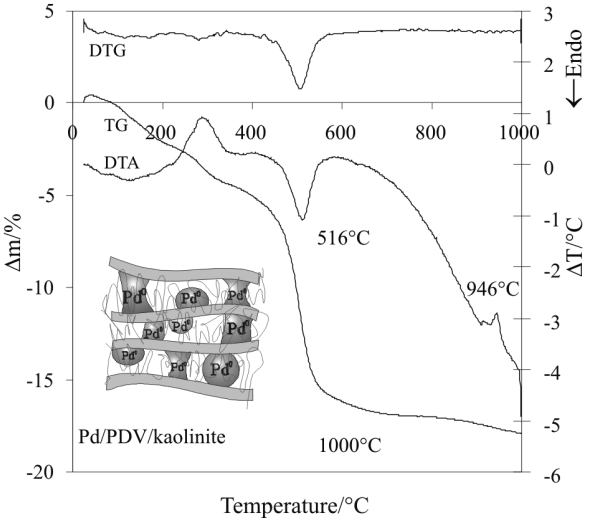

Fig. 12b The TG and DTA curves of palladium (1 mass%)/PVP/ kaolinite nanocomposite

taining non-ionic PVP display relatively small, nearly monodisperse particles, which tend to stick together when the polymer concentration is increased.

Figure 11a demonstrates the endothermic peak characteristic of the dehydration of pure kaolinite, followed by dehydroxylation characteristic of structural change at 450–550°C.

The incorporation of DMSO, leading to disaggregation of kaolinite is clearly confirmed by thermoanalysis (Fig. 11b). DMSO intercalated in the interlamellar space is removed at 190–220°C. When surfactants or polymers are adsorbed on nanoparticles for stabilization, these organic molecules are oxidized in air at ca. 290–300°C (Fig. 12 a,b). The presence of metallic palladium is not detectable due to its low amount (1 mass%) as well as its high melting point (1200°C).

References

1 C.-C. Wang and J. Y. Ying, Chem. Mater., 11 (1999) 3113.
2 J. Sterte, Clays and Clay Minerals, 34 (1986) 658.
3 H. Yoneyama, S. Haga and S. Yamanaka, J. Phys. Chem., 93 (1989) 4833.
4 A. Bernier, L. F. Admaiai and P. Grange, Appl. Catal., 77 (1991) 269.
5 C. Ooka, S. Akita, Y. Ohashi, T. Horiuchi, K. Suzuki, S.-i. Komai, H. Yoshida and T. Hattori, J. Mat. Chem., 9 (1999) 2943.
6 L. Spanhel and M. A. Anderson, J. Am. Chem. Soc., 113 (1991) 2833.
7 D. W. Bahnemann, C. Kormann and M. R. Hoffmann, J. Phys. Chem., 91 (1987) 3789.

8 Z. Hu, S. Chen and S. Peng, J. Colloid Interface Sci., 182 (1996) 457.
9 Y. Inubushi, R. Takami, M. Iwasaki, H. Tada and S. Ito, J. Colloid Interface Sci., 200 (1998) 220.
10 A. Taubert, G. Glasser and D. Palms, Langmuir, 18 (2002) 4488.
11 D. Kaneko, H. Shouji, T. Kawai and K. Kon-No, Langmuir, 16 (2000) 4086.
12 C. L. Carnes and K. J. Klabunde, Langmuir, 16 (2000) 3764.
13 S. G. Ansari, P. Boroojerdian, S. R. Sainkar, R. N. Karekar, R. C. Aiyer and S. K. Kulkarni, Thin Solid Films, 295 (1997) 271.
14 S. Chappel and A. Zaban, Solar Energy Materials and Solar Cells, 71 (2002) 141.
15 W. Cun, Z. Jincai, W. Xinming, M. Bixian, S. Gouying, P. Ping'an and F. Jiamo, Applied Catalysis B, Environmental, 39 (2002) 269.
16 I. Dékány, L. Turi, E. Tombácz and J. H. Fendler, Langmuir, 11 (1995) 2285.
17 I. Kiricsi, I. Pálinkó, Gy. Tasi and I. Hannus, Molecular Crystals and Liqud Crystals, 244 (1994) 149.
18 V. M. Jiménez, A. R. Gonzalez Elipe, J. P. Espinos, A. Justo and A. Fernandez, Sensors and Actuators B, 31 (1996) 29.
19 Z. Ding, H. Y. Zhu, G. Q. Lu and P. F. Greenfield, J. Colloid Interface Sci., 209 (1999) 193.
20 I. Dékány, L. Turi, A. Szűcs and Z. Király, Coll. Surf. A, 141 (1998) 405.
21 A. Szűcs, Z. Király, F. Berger and I. Dékány, Coll. Surf. A, 139 (1998) 109.
22 S. Papp, A. Szűcs and I. Dékány, Appl. Clay Sci., 19 (2001) 155.
23 S. Papp, A. Szűcs and I. Dékány, Solid State Ionics, 141–142 (2001) 169.
24 K. Mogyorósi, I. Dékány and J. H. Fendler, Langmuir, 19 (2003) 2938.